Electromagnetic Scattering from 3-D Curved Dielectric Bodies Using Time-Domain Integral Equations

Martin D. Pocock, Michael J. Bluck, and Simon P. Walker

***Abstract*— A boundary integral equation (BIE) approach is developed to calculate transient scattering from dielectric bodies. The treatment is directly in terms of the E and H fields rather than magnetic and electric currents. It employs curvilinear (quadratic) modeling, which allows accurate representation of arbitrarily shaped curved bodies. The treatment is isoparametric with the same quadratic representation of the spatial field variation and with the temporal variation modeled by similar quadratic elements. Integration employs high-order Gaussian quadrature with special treatment of the singular and hypersingular integrals that arise. The treatment is implicit, requiring the solution of a sparse matrix equation at each timestep. This adds only trivially to the cost at each timestep and, by freeing the timestep from the constraint that it be smaller than the smallest nodal spacing, can greatly reduce the number of timesteps that must be employed. Additionally, it produces stable results without resort to the averaging processes proposed elsewhere. Example calculations of scattering from a sphere, a cube, and an almond are presented and compared with earlier published transient results and with results from a frequency domain treatment. Good agreement and improved accuracy is found.**

***Index Terms*—Electromagnetic scattering, transient scattering.**

I. Introduction

In this paper, we describe a boundary integral equation (BIE) technique for the time-domain solution of scattering from three-dimensional (3-D) dielectric bodies. The BIE method employed uses numerical treatments which are more common in areas such as elastostatics, but are as yet little used in electrodynamics. They include curvilinear modeling of the geometry and isoparametric quadratic representation of the field spatial and temporal variation with high-order Gaussian quadrature and special integration techniques for singular integrands. The treatment is implicit, both gaining considerable computational economies and avoiding the stability problems which explicit treatments exhibit.

A review of the range of methods used for electromagnetic field modeling has been published by Miller [1]. Here we are concerned with integral methods applied to 3-D time-domain systems of which there are relatively few occurrences in the literature [2]–[5] (compared to say integral-equation frequency-domain or finite-difference time-domain analyses). Of these, a small number [6]–[8] have addressed dielectric bodies.

In their paper, Mieras and Bennett (1982) [6] use a flat facetted representation of the geometry coupled with piecewise constant approximation of field and Green function. Integrals over self patches were evaluated analytically. An explicit solution scheme was used with the timestep constrained so that the field at any location could be expressed as a summation of known historical field values. Instabilities were observed.

In 1994, Rynne [7] presented computations of scattering from dielectric targets using essentially the same numerical formulation as Mieras and Bennett in 1982. Two techniques are used in combination to suppress exponentially growing instabilities. The natural approximation to the time derivative of the form $f' = (f^{k+1} - f^k)/\Delta t$ is replaced by the less accurate $f' = (f^{k+1} - f^{k-1})/2\Delta t$. In addition, a retrospective time averaging $f^k = (f^{k+1} + 2f^k + f^{k-1})/4$ is applied. These incorporations of earlier values reduce the accuracy somewhat, but their use of information from an earlier timestep has the effect of helping to cancel the oscillatory instability.

Also in 1994, Vechinski *et al.* [8] use the common Rao–Wilton–Glisson elements [9] to represent geometry and field. These are, again, planar triangles with enforced edge-current continuity. Again, late-time stability is a problem and an averaging technique is applied to suppress the instabilities.

As has been seen, the normal treatment in the time domain is to force the equations to become explicit; that is, at each time step, each unknown value can be written wholly in terms of "known" values, which have been determined at previous time steps. Besides leading to stability problems, this restricts the choice of time-step size to less then the smallest spatial discretization. In practice, it is often desirable to use a mesh that is very fine over some portions of the body to model sharp geometric variation (such as the NASA almond [10], which will be used later as an example), while elsewhere the mesh fineness is determined only by the need to represent the field adequately. In such circumstances, explicit methods require time steps to be constrained to suit this geometrical refinement, rather than be small enough only to model the temporal variation of the field. The consequence can be a very marked increase in cost, which the more general implicit approach avoids.

In formulating the integral equations, the equivalence principle [11] is applied. This usually results in a matrix system

Manuscript received July 17, 1996; revised September 30, 1997. This work was supported by British Aerospace, the Ministry of Defence, the Engineering and Physical Sciences Research Council and the Medical Research Council.

The authors are with the Computational Mechanics Section, Mechanical Engineering Department, Imperial College of Science Technology and Medicine, London, SW7 2BX U.K.

Publisher Item Identifier S 0018-926X(98)06104-3.

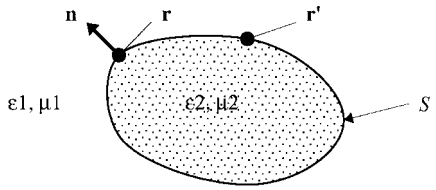

Fig. 1. Notation used for dielectric bodies. The body parameters have subscript "2" and the surrounding space "1"; the normal $\mathbf{n}$ is directed away from the body and $\mathbf{r}$ and $\mathbf{r}'$ represent two points on the body's surface S.

in terms of tangential surface currents ($\mathbf{J}$ and $\mathbf{M}$) and the normal components of the $\mathbf{E}$- and $\mathbf{H}$-fields. Here, the integral equations are formulated directly in terms of the $\mathbf{E}$ and $\mathbf{H}$ fields. This use of the Cartesian components of the fields eases agglomerating the matrix and vector coefficients.

In Section II we present the algebraic formulation. Section III describes method for forming and subsequently solving the matrix system. The effectiveness of the present approach is demonstrated in Section IV, where a comparison is made with previously published results.

II. Algebraic Formulation

The problem considered here consists of a (lossless, isotropic) body with dielectric properties different from those of the surrounding space. The notation used is represented in Fig. 1: the body parameters have subscript "2" and the surrounding space "1"; the normal $\mathbf{n}$ is directed away from the body and $\mathbf{r}$ and $\mathbf{r}'$ represent two points on the body's surface S.

Integral equations are derived from the Maxwell equations [12]. The exterior region equations are

$$\alpha_1\mathbf{E}_1 = \mathbf{E}^{\text{inc}} + \frac{1}{4\pi}\int_S \left\{ -\frac{\mu_1}{R}\mathbf{n}'\times\frac{\partial\mathbf{H}_1'}{\partial t^*} + \left(\frac{1}{R}\mathbf{n}'\times\mathbf{E}_1' + \frac{1}{c_1}\mathbf{n}'\times\frac{\partial\mathbf{E}_1'}{\partial t^*}\right)\times\frac{\hat{\mathbf{R}}}{R} + \left(\frac{1}{R}\mathbf{n}'\cdot\mathbf{E}_1' + \frac{1}{c_1}\mathbf{n}'\cdot\frac{\partial\mathbf{E}_1'}{\partial t^*}\right)\frac{\hat{\mathbf{R}}}{R}\right\} ds' \quad (1)$$

$$\alpha_1\mathbf{H}_1 = \mathbf{H}^{\text{inc}} + \frac{1}{4\pi}\int_S \left\{ \frac{\varepsilon_1}{R}\mathbf{n}'\times\frac{\partial\mathbf{E}_1'}{\partial t^*} + \left(\frac{1}{R}\mathbf{n}'\times\mathbf{H}_1' + \frac{1}{c_1}\mathbf{n}'\times\frac{\partial\mathbf{H}_1'}{\partial t^*}\right)\times\frac{\hat{\mathbf{R}}}{R} + \left(\frac{1}{R}\mathbf{n}'\cdot\mathbf{H}_1' + \frac{1}{c_1}\mathbf{n}'\cdot\frac{\partial\mathbf{E}_1'}{\partial t^*}\right)\frac{\hat{\mathbf{R}}}{R}\right\} ds' \quad (2)$$

and the interior equations

$$\alpha_2\mathbf{E}_2 = -\frac{1}{4\pi}\int_S \left\{ -\frac{\mu_2}{R}\mathbf{n}'\times\frac{\partial\mathbf{H}_2'}{\partial t^*} + \left(\frac{1}{R}\mathbf{n}'\times\mathbf{E}_2' + \frac{1}{c_2}\mathbf{n}'\times\frac{\partial\mathbf{E}_2'}{\partial t^*}\right)\times\frac{\hat{\mathbf{R}}}{R} + \left(\frac{1}{R}\mathbf{n}'\cdot\mathbf{E}_2' + \frac{1}{c_2}\mathbf{n}'\cdot\frac{\partial\mathbf{E}_2'}{\partial t^*}\right)\frac{\hat{\mathbf{R}}}{R}\right\} ds' \quad (3)$$

$$\alpha_2\mathbf{H}_2 = -\frac{1}{4\pi}\int_S \left\{ \frac{\varepsilon_2}{R}\mathbf{n}'\times\frac{\partial\mathbf{E}_2'}{\partial t^*} + \left(\frac{1}{R}\mathbf{n}'\times\mathbf{H}_2' + \frac{1}{c_2}\mathbf{n}'\times\frac{\partial\mathbf{H}_2'}{\partial t^*}\right)\times\frac{\hat{\mathbf{R}}}{R} + \left(\frac{1}{R}\mathbf{n}'\cdot\mathbf{H}_2' + \frac{1}{c_2}\mathbf{n}'\cdot\frac{\partial\mathbf{H}_2'}{\partial t^*}\right)\frac{\hat{\mathbf{R}}}{R}\right\} ds'. \quad (4)$$

Here, the retarded time is $t^* = t - R/c_i$ and α_i is the solid angle subtended at the field location with i representing region one (exterior) or two (interior).

The integral equations are combined using the appropriate interface conditions

$$\mathbf{n}\cdot(\mathbf{D}_1 - \mathbf{D}_2) = 0, \qquad \mathbf{n}\cdot(\mathbf{B}_1 - \mathbf{B}_2) = 0$$
$$\mathbf{n}\times(\mathbf{E}_1 - \mathbf{E}_2) = 0, \qquad \mathbf{n}\times(\mathbf{H}_1 - \mathbf{H}_2) = 0. \quad (5a\text{–}d)$$

These interface conditions are used to eliminate (for example) the interior fields (subscript "2") from the right-hand-side integral equations (3) and (4). The vector identity $\mathbf{V} \equiv \mathbf{n}(\mathbf{n}\cdot\mathbf{V}) - \mathbf{n}\times(\mathbf{n}\times\mathbf{V})$ is used to eliminate the interior fields from the left-hand side of these equations. Thus, the interior $\mathbf{E}$- and $\mathbf{H}$-field equations can be written in terms of the exterior fields as

$$\alpha_2\left[\frac{\varepsilon_1}{\varepsilon_2}\mathbf{n}(\mathbf{n}\cdot\mathbf{E}_1) - \mathbf{n}\times(\mathbf{n}\times\mathbf{E}_1)\right] = -\frac{1}{4\pi}\int_S \left\{ \left(-\frac{\mu_2}{R}\mathbf{n}'\times\frac{\partial\mathbf{H}_1'}{\partial t^*}\right) + (\mathbf{n}'\times\mathbf{E}_1')\times\frac{\hat{\mathbf{R}}}{R^2} + \frac{1}{c_2}\left(\mathbf{n}'\times\frac{\partial\mathbf{E}_1'}{\partial t^*}\right)\times\frac{\hat{\mathbf{R}}}{R} + \frac{\varepsilon_1}{\varepsilon_2}\mathbf{n}'\cdot\mathbf{E}_1'\frac{\hat{\mathbf{R}}}{R^2} + \frac{\varepsilon_1}{\varepsilon_2}\frac{1}{c_2}\mathbf{n}'\cdot\frac{\partial\mathbf{E}_1'}{\partial t^*}\frac{\hat{\mathbf{R}}}{R}\right\} ds' \quad (6)$$

$$\alpha_2\left[\frac{\mu_1}{\mu_2}\mathbf{n}(\mathbf{n}\cdot\mathbf{H}_1) - \mathbf{n}\times(\mathbf{n}\times\mathbf{H}_1)\right] = -\frac{1}{4\pi}\int_S \left\{ \frac{\varepsilon_2}{R}\mathbf{n}'\times\frac{\partial\mathbf{E}_1'}{\partial t^*} + (\mathbf{n}'\times\mathbf{H}_1')\times\frac{\hat{\mathbf{R}}}{R^2} + \frac{1}{c_2}\left(\mathbf{n}'\times\frac{\partial\mathbf{H}_1'}{\partial t^*}\right)\times\frac{\hat{\mathbf{R}}}{R} + \frac{\mu_1}{\mu_2}\mathbf{n}'\cdot\mathbf{H}_1'\frac{\hat{\mathbf{R}}}{R^2} + \frac{\mu_1}{\mu_2}\frac{1}{c_2}\mathbf{n}'\cdot\frac{\partial\mathbf{H}_1'}{\partial t^*}\frac{\hat{\mathbf{R}}}{R}\right\} ds'. \quad (7)$$

Several authors [6], [7] have discussed methods for combining the exterior (1) and (2) and interior (6) and (7) equations. In essence, these various alternatives comprise the addition of some multiple of one equation to the other. Mieras and Bennett [6] found a particular choice was required to help suppress instabilities. We have found it sufficient simply to add the equations with equal weights (and indeed have not investigated alternatives.

The equations to be discretised and subsequently solved are, therefore

$$\alpha_1\mathbf{E}_1+\alpha_2\left[\frac{\varepsilon_1}{\varepsilon_2}\mathbf{n}(\mathbf{n}\cdot\mathbf{E}_1)-\mathbf{n}\times(\mathbf{n}\times\mathbf{E}_1)\right]$$
$$=\mathbf{E}^{\text{inc}}+\frac{1}{4\pi}\int_S\left\{\left(-\frac{\mu_1}{R}\mathbf{n}'\times\frac{\partial\mathbf{H}_1'}{\partial t^*}\right)+(\mathbf{n}'\times\mathbf{E}_1')\times\frac{\hat{\mathbf{R}}}{R^2}+\frac{1}{c_1}\left(\mathbf{n}'\times\frac{\partial\mathbf{E}_1'}{\partial t^*}\right)\times\frac{\hat{\mathbf{R}}}{R}+\mathbf{n}'\cdot\mathbf{E}_1'\frac{\hat{\mathbf{R}}}{R^2}+\frac{1}{c_1}\mathbf{n}'\cdot\frac{\partial\mathbf{E}_1'}{\partial t^*}\frac{\hat{\mathbf{R}}}{R}\right\}ds'$$
$$-\frac{1}{4\pi}\int_S\left\{\left(-\frac{\mu_2}{R}\mathbf{n}'\times\frac{\partial\mathbf{H}_1'}{\partial t^*}\right)+(\mathbf{n}'\times\mathbf{E}_1')\times\frac{\hat{\mathbf{R}}}{R^2}+\frac{1}{c_2}\left(\mathbf{n}'\times\frac{\partial\mathbf{E}_1'}{\partial t^*}\right)\times\frac{\hat{\mathbf{R}}}{R}+\frac{\varepsilon_1}{\varepsilon_2}\mathbf{n}'\cdot\mathbf{E}_1'\frac{\hat{\mathbf{R}}}{R^2}+\frac{\varepsilon_1}{\varepsilon_2}\frac{1}{c_2}\mathbf{n}'\cdot\frac{\partial\mathbf{E}_1'}{\partial t^*}\frac{\hat{\mathbf{R}}}{R}\right\}ds' \tag{8}$$

$$\alpha_1\mathbf{H}_1+\alpha_2\left[\frac{\varepsilon_1}{\varepsilon_2}\mathbf{n}(\mathbf{n}\cdot\mathbf{H}_1)-\mathbf{n}\times(\mathbf{n}\times\mathbf{H}_1)\right]$$
$$=\mathbf{H}^{\text{inc}}+\frac{1}{4\pi}\int_S\left\{\left(\frac{\varepsilon_1}{R}\mathbf{n}'\times\frac{\partial\mathbf{E}_1'}{\partial t^*}\right)+(\mathbf{n}'\times\mathbf{H}_1')\times\frac{\hat{\mathbf{R}}}{R^2}+\frac{1}{c_1}\left(\mathbf{n}'\times\frac{\partial\mathbf{H}_1'}{\partial t^*}\right)\times\frac{\hat{\mathbf{R}}}{R}+\mathbf{n}'\cdot\mathbf{H}_1'\frac{\hat{\mathbf{R}}}{R^2}+\frac{1}{c_1}\mathbf{n}'\cdot\frac{\partial\mathbf{H}_1'}{\partial t^*}\frac{\hat{\mathbf{R}}}{R}\right\}ds'$$
$$-\frac{1}{4\pi}\int_S\left\{\left(\frac{\varepsilon_2}{R}\mathbf{n}'\times\frac{\partial\mathbf{E}_1'}{\partial t^*}\right)+(\mathbf{n}'\times\mathbf{H}_1')\times\frac{\hat{\mathbf{R}}}{R^2}+\frac{1}{c_2}\left(\mathbf{n}'\times\frac{\partial\mathbf{H}_1'}{\partial t^*}\right)\times\frac{\hat{\mathbf{R}}}{R}+\frac{\mu_1}{\mu_2}\mathbf{n}'\cdot\mathbf{H}_1'\frac{\hat{\mathbf{R}}}{R^2}+\frac{\mu_1}{\mu_2}\frac{1}{c_2}\mathbf{n}'\cdot\frac{\partial\mathbf{H}_1'}{\partial t^*}\frac{\hat{\mathbf{R}}}{R}\right\}ds'. \tag{9}$$

Equations (8) and (9) may be contrasted with Rynne [7, eqs. (2.9) and (2.10)], where the more common surface electric and magnetic currents are used. In addition, Rynne leaves the choice of coupling weights free.

Discretization of the Integral Equations: This work is an extension of the perfectly conducting BIE approach described by Bluck and Walker [5]. We employ isoparametric quadratic discretization with nine-noded Lagrangian elements and point collocation. Temporally, piecewise quadratic interpolation is used. The radial distance vector from the ith spatial node (with location $\mathbf{r}_i$) to the (ξ,η) coordinate location on the mth spatial element is written as

$$\mathbf{R}_m(\mathbf{r}_i;\xi,\eta)=\mathbf{r}_i-\sum_{\alpha=1}^{9}S_\alpha(\xi,\eta)\mathbf{r}_{m,\alpha} \tag{10}$$

where S_α is the αth spatial shape function and $\mathbf{r}_{m,\alpha}$ is the position vector of the αth local node on the mth spatial element. The actual form of the spatial shape functions are described in many finite-element texts.

The spatial variation of E field over the element m, at the retarded time t^* (where $t^*=t-R/c$) can be written as

$$\mathbf{E}(\xi,\eta;t^*)\big|_m=\sum_{\alpha=1}^{9}S_\alpha(\xi,\eta)\mathbf{E}_{\alpha,m}(t^*). \tag{11}$$

Here, $\mathbf{E}_{\alpha,m}$ represents the $\mathbf{E}$ field at the αth node of spatial element m. The temporal variation of the $\mathbf{E}$ field at the nodal location (α,m) can be described by

$$\mathbf{E}_{\alpha,m}(t^*)=\sum_{\beta=1}^{3}T_\beta(\tau)\mathbf{E}_{\alpha,m}^{\beta,p^*}. \tag{12}$$

Here, T is the temporal shape function and $\mathbf{E}_{\alpha,m}^{\beta,p^*}$ represents the $\mathbf{E}$ field at the αth node of spatial element m and the βth node of time element p^*.

The number of time elements ago, identifying the temporal element in which the retarded time falls, is given by

$$p^*=\text{int}\left\{\frac{R}{2c\Delta t}\right\}+1 \tag{13}$$

(where Δt is the time step size) and the intrinsic time coordinate is determined from

$$\tau=2p^*-1-\frac{R}{c\Delta t}. \tag{14}$$

Integration over the quadratic elements is by Gaussian quadrature. The number of quadrature points used per element can be varied from four to over four hundred depending on the geometry and accuracy required; 36 quadrature locations per element have been used for the examples given later.

When the field node and source element coincide the variation of the integrand is so rapid that special integration techniques are required. Both weakly singular $(1/R)$ and strongly singular $(1/R^2)$ kernels must be treated. (It is noted that although the integral equations for perfectly conducting bodies also contain order $(1/R)$ and $(1/R^2)$ singularities, the $(1/R^2)$ is weakened to $(1/R)$ for smooth surfaces.) The weakly singular kernels are integrated by a repartitioning technique based on Lachat and Watson [13]. For strongly singular, "Cauchy principal value" integrations, a method incorporating subtraction of the singularity via "tangent planes" has been developed. This is an extension of the methods developed for the treatment of these terms for perfect conductors [14].

The discretization is discussed more fully elsewhere [5], [15], [16]. The discretized equations can be written as

$$\alpha_1\mathbf{E}+\alpha_2\left[\frac{\varepsilon_1}{\varepsilon_2}\mathbf{n}(\mathbf{n}\cdot\mathbf{E})-\mathbf{n}\times(\mathbf{n}\times\mathbf{E})\right]$$
$$=\mathbf{E}^{\text{inc}}+\frac{1}{4\pi}\sum_{m=1}^{M}\sum_{q}|J|\omega_q\sum_{\alpha=1}^{9}\sum_{\beta=1}^{3}S_\alpha\left[\frac{\dot{T}_\beta(\tau(R))}{\Delta t}\times\left[-\frac{\mu_1}{R}\mathbf{n}'\times\mathbf{H}_{\alpha,m}^{\beta,p^*}+\frac{1}{c_1}(\mathbf{n}'\times\mathbf{E}_{\alpha,m}^{\beta,p^*})\times\frac{\hat{\mathbf{R}}}{R}+\frac{1}{c_1}(\mathbf{n}'\cdot\mathbf{E}_{\alpha,m}^{\beta,p^*})\frac{\hat{\mathbf{R}}}{R}\right]+T_\beta(\tau(R))\left[(\mathbf{n}'\times\mathbf{E}_{\alpha,m}^{\beta,p^*})\times\frac{\hat{\mathbf{R}}}{R^2}+(\mathbf{n}'\cdot\mathbf{E}_{\alpha,m}^{\beta,p^*})\frac{\hat{\mathbf{R}}}{R^2}\right]\right] \tag{15}$$

$$
\begin{aligned}
&- \frac{1}{4\pi}\sum_{m=1}^{M}\sum_{q}|J|\omega_q\sum_{\alpha=1}^{9}\sum_{\beta=1}^{3}S_\alpha\left[\frac{\dot{T}_\beta(\tau(R))}{\Delta t}\right.\\
&\times\left[-\frac{\mu_2}{R}\mathbf{n}'\times\mathbf{H}_{\alpha,m}^{\beta,p^*}+\frac{1}{c_2}\left(\mathbf{n}'\times\mathbf{E}_{\alpha,m}^{\beta,p^*}\right)\times\frac{\hat{\mathbf{R}}}{R}\right.\\
&\quad\left.+\frac{\varepsilon_1}{\varepsilon_2}\frac{1}{c_2}\left(\mathbf{n}'\cdot\mathbf{E}_{\alpha,m}^{\beta,p^*}\right)\frac{\hat{\mathbf{R}}}{R}\right]+T_\beta(\tau(R))\Big[\left(\mathbf{n}'\times\mathbf{E}_{\alpha,m}^{\beta,p^*}\right)\\
&\quad\times\left.\left.\frac{\hat{\mathbf{R}}}{R^2}+\frac{\varepsilon_1}{\varepsilon_2}\left(\mathbf{n}'\times\mathbf{E}_{\alpha,m}^{\beta,p^*}\right)\frac{\hat{\mathbf{R}}}{R^2}\right]\right]
\end{aligned}
$$

$$
\begin{aligned}
&\alpha_1\mathbf{H}_1+\alpha_2\left[\frac{\varepsilon_1}{\varepsilon_2}\mathbf{n}(\mathbf{n}\cdot\mathbf{H}_1)-\mathbf{n}\times(\mathbf{n}\times\mathbf{H}_1)\right]\\
&\quad=\mathbf{H}^{\text{inc}}+\frac{1}{4\pi}\sum_{m=1}^{M}\sum_{q}|J|\omega_q\sum_{\alpha=1}^{9}\sum_{\beta=1}^{3}S_\alpha\left[\frac{\dot{T}_\beta(\tau(R))}{\Delta t}\right.\\
&\qquad\times\left[\frac{\varepsilon_1}{R}\mathbf{n}'\times\mathbf{E}_{\alpha,m}^{\beta,p^*}+\frac{1}{c_1}\left(\mathbf{n}'\times\mathbf{H}_{\alpha,m}^{\beta,p^*}\right)\right.\\
&\qquad\left.\times\frac{\hat{\mathbf{R}}}{R}+\frac{1}{c_1}\left(\mathbf{n}'\cdot\mathbf{H}_{\alpha,m}^{\beta,p^*}\right)\frac{\hat{\mathbf{R}}}{R}\right]+T_\beta(\tau(R))\\
&\qquad\times\left.\left[\left(\mathbf{n}'\times\mathbf{H}_{\alpha,m}^{\beta,p^*}\right)\times\frac{\hat{\mathbf{R}}}{R^2}+\left(\mathbf{n}'\cdot\mathbf{H}_{\alpha,m}^{\beta,p^*}\right)\frac{\hat{\mathbf{R}}}{R^2}\right]\right]\\
&\qquad-\frac{1}{4\pi}\sum_{m=1}^{M}\sum_{q}|J|\omega_q\sum_{\alpha=1}^{9}\sum_{\beta=1}^{3}S_\alpha\left[\frac{\dot{T}_\beta(\tau(R))}{\Delta t}\right.\\
&\qquad\times\left[\frac{\varepsilon_1}{R}\mathbf{n}'\times\mathbf{E}_{\alpha,m}^{\beta,p^*}+\frac{1}{c_2}\left(\mathbf{n}'\times\mathbf{H}_{\alpha,m}^{\beta,p^*}\right)\times\frac{\hat{\mathbf{R}}}{R}\right.\\
&\qquad\left.+\frac{\mu_1}{\mu_2}\frac{1}{c_2}\left(\mathbf{n}'\cdot\mathbf{H}_{\alpha,m}^{\beta,p^*}\right)\frac{\hat{\mathbf{R}}}{R}\right]+T_\beta(\tau(R))\\
&\qquad\times\left.\left.\left[\left(\mathbf{n}'\times\mathbf{H}_{\alpha,m}^{\beta,p^*}\right)\times\frac{\hat{\mathbf{R}}}{R^2}+\frac{\mu_1}{\mu_2}\left(\mathbf{n}'\times\mathbf{H}_{\alpha,m}^{\beta,p^*}\right)\frac{\hat{\mathbf{R}}}{R^2}\right]\right]\right.. \qquad (16)
\end{aligned}
$$

The summations are over the M elements; (usually) for 36 quadrature locations, q, over nine nodes per spatial element and three per temporal element. The Jacobian of the transform to the bi-unit square is $|J|$ and ω_q is the Gaussian quadrature weight corresponding to Gauss location q. Here, $\mathbf{E}_{\alpha,m}^{\beta,p^*}$ represents the E field at the αth node of spatial element m and the βth node of time element p^* ago. The dependence on parameterised quadrature locations and field location has been suppressed for clarity. In full, the radial vector R, for example would be written as $R_m(\mathbf{r}_i;(\xi,\eta)_q)$.

Formation and Solution of the Matrix System: We now address the manipulations required to develop a soluble matrix system from (15) and (16). To create a matrix which multiplies the solution vector (of $\mathbf{E}$ and $\mathbf{H}$ fields) the following 3×3 matrices (tensors) are defined:

$$
[A]\mathbf{V}\equiv(\mathbf{n}\times\mathbf{V})\times\mathbf{R};\qquad [B]\mathbf{V}\equiv\mathbf{n}\times\mathbf{V}
$$
$$
[C]\mathbf{V}\equiv(\mathbf{n}\cdot\mathbf{V})\mathbf{R}. \qquad (17a\text{–}c)
$$

Written in component form the $[A]$ matrix, for example, is

$$
[A]=\begin{bmatrix} n_2R_2+n_3R_3 & -n_1R_2 & -n_1R_3\\ -n_2R_1 & n_1R_1+n_3R_3 & -n_2R_3\\ -n_3R_1 & -n_3R_2 & n_1R_1+n_2R_2\end{bmatrix}. \qquad (18)
$$

Using these matrices, the $\mathbf{E}$ field (17) is written as below (and the $\mathbf{H}$ field (16) follows similarly):

$$
\begin{aligned}
&\alpha_1\mathbf{E}+\alpha_2\left[\frac{\varepsilon_1}{\varepsilon_2}\mathbf{n}(\mathbf{n}\cdot\mathbf{E})-\mathbf{n}\times(\mathbf{n}\times\mathbf{E})\right]\\
&\quad=\mathbf{E}^{\text{inc}}+\frac{1}{4\pi}\sum_{m=1}^{M}\sum_{q}|J|\omega_q\sum_{\alpha=1}^{9}\sum_{\beta=1}^{3}S_\alpha\\
&\qquad\times\left\{\left(\frac{\dot{T}_\beta(\tau(R))}{\Delta t}\frac{1}{c_1R}+T_\beta(\tau(R))\frac{1}{R^2}\right)[A]\mathbf{E}_{\alpha,m}^{\beta,p^*}\right.\\
&\qquad\quad+\left(\frac{\dot{T}_\beta(\tau(R))}{\Delta t}\frac{1}{c_1R}+T_\beta(\tau(R))\frac{1}{R^2}\right)[C]\mathbf{E}_{\alpha,m}^{\beta,p^*}\\
&\qquad\quad\left.-\left(\frac{\dot{T}_\beta(\tau(R))}{\Delta t}\frac{\mu_1}{R}\right)[B]\mathbf{H}_{\alpha,m}^{\beta,p^*}\right\} \qquad (19)\\
&\qquad-\frac{1}{4\pi}\sum_{m=1}^{M}\sum_{q}|J|\omega_q\sum_{\alpha=1}^{9}\sum_{\beta=1}^{3}S_\alpha\\
&\qquad\times\left\{\left(\frac{\dot{T}_\beta(\tau(R))}{\Delta t}\frac{1}{c_2R}+T_\beta(\tau(R))\frac{1}{R^2}\right)[A]\mathbf{E}_{\alpha,m}^{\beta,p^*}\right.\\
&\qquad\quad+\frac{\varepsilon_1}{\varepsilon_2}\left(\frac{\dot{T}_\beta(\tau(R))}{\Delta t}\frac{1}{c_2R}+T_\beta(\tau(R))\frac{1}{R^2}\right)[C]\mathbf{E}_{\alpha,m}^{\beta,p^*}\\
&\qquad\quad\left.-\left(\frac{\dot{T}_\beta(\tau(R))}{\Delta t}\frac{\mu_2}{R}\right)[B]\mathbf{H}_{\alpha,m}^{\beta,p^*}\right\}.
\end{aligned}
$$

As noted, the formulation here is directly in terms of the E and H fields: the common formulation is for tangential surface field (**J** and **M**) and normal scalar field (**n**.**E** and **n**.**H**) equations. Due to the **E**- and **H**-field formulation, each of the unknowns can be written in terms of their Cartesian components, which makes for easier combination into a matrix system.

Writing the six-vector comprising the Cartesian components of $\mathbf{E}$ and $\mathbf{H}$ as

$$
\begin{Bmatrix}\mathbf{E}\\ \mathbf{H}\end{Bmatrix}=\begin{bmatrix}E_x\\ E_y\\ E_z\\ H_x\\ H_y\\ H_z\end{bmatrix} \qquad (20)
$$

the discretised integral equation can be written as

$$
\begin{aligned}
&\alpha_1\begin{Bmatrix}\mathbf{E}\\ \mathbf{H}\end{Bmatrix}+\alpha_2\begin{Bmatrix}\frac{\varepsilon_1}{\varepsilon_2}\mathbf{n}(\mathbf{n}\cdot\mathbf{E})\\ \frac{\mu_1}{\mu_2}\mathbf{n}(\mathbf{n}\cdot\mathbf{H})\end{Bmatrix}-\alpha_2\begin{Bmatrix}\mathbf{n}\times\mathbf{n}(\mathbf{n}\cdot\mathbf{E})\\ \mathbf{n}\times(\mathbf{n}\times\mathbf{H})\end{Bmatrix}\\
&\quad=\begin{Bmatrix}\mathbf{E}\\ \mathbf{H}\end{Bmatrix}^{\text{inc}}+\sum_{m=1}^{M}\sum_{q}\sum_{\alpha=1}^{9}\sum_{\beta=1}^{3}[K]\begin{Bmatrix}\mathbf{E}\\ \mathbf{H}\end{Bmatrix}_{\alpha,m}^{\beta,p^*} \qquad (21)
\end{aligned}
$$

where $[K]$ is the amalgamation of the right-hand sides of (19) and its $\mathbf{H}$-field equivalent.

Implicitness and Stability: It can be seen from the integral equations that the field at the present location and time is calculated from the fields at points on the surface at the relevant retarded times. Many of these retarded time values will have been determined at previous time steps. It is only the nearby field contributions that are influenced by as yet undetermined field values. Nearby in this context means nodes with associated Gauss point locations within the support of the temporal shape function; that is, within a sphere of radius $2c\Delta t$ of the field node.

Coefficients multiplying these known values are multiplied by the corresponding retarded surface field values and added to the incident field to obtain the right-hand-side vector for the matrix system. Coefficients multiplying as yet unknown values remain on the left-hand side, forming a sparse matrix. Solution of this sparse system is performed at each time step. The actual matrix solution is achieved at negligible computational cost using an iterative solver. The dominant cost, just as with the explicit approach, are the summations required to form the right-hand sides of (21) at each timestep. These issues of storage and operation requirements are discussed more fully elsewhere [5], [16], [17].

It is observed that this implicit approach provides stability, and we have found no need to apply the various stabilization schemes [7], [8] noted above, which are used with the more common explicit, "marching on in time" methods.

III. Results

We present below several example results obtained with the method described. The geometries used are a sphere, a cube, and the NASA almond [10].

A. Sphere

Vechinski *et al*. [8] publish results for a dielectric sphere and compare with an analytical result. The unit radius sphere is centered at the coordinate origin and is of properties $\varepsilon_{r2} = 2.0$ $\mu_{r2} = 1.0$. The incident pulse is described by

$$\mathbf{E}^{\text{inc}} = \mathbf{E}_0 \frac{1}{\sqrt{\pi}} e^{[-(ct - ct_0 - \mathbf{r}\cdot\hat{\mathbf{k}})^2]}$$

with $\mathbf{E}_0 = \mathbf{u}_x$, $\hat{\mathbf{k}} = -\mathbf{u}_z$ and the initial wave origin set by $ct_0 = 6.0$. The triad $(\mathbf{u}_x, \mathbf{u}_y, \mathbf{u}_z)$ represent the unit vectors in the coordinate directions.

Vechinski *et al*. [8] use 138 Rao–Wilton–Glisson [9] patches (a total of 207 edges) to describe the sphere and the surface fields. The BIE results presented here use 24 nine-noded quadratic quadrilateral elements (98 nodes).

We define the usual spherical-polar coordinate system (r, θ, ϕ) relative to the $(\mathbf{u}_x, \mathbf{u}_y, \mathbf{u}_z)$ triad. Fig. 2 shows the equivalent surface magnetic current, M_ϕ at $\theta = 90°$, $\phi = 0°$, and Fig. 3 shows the equivalent surface electric current J_ϕ at $\theta = 90°$, $\phi = 90°$. Of the four surface currents presented in Vechinski *et al*., these are the two which display greatest differences between the computed and analytical results. It can be seen from the graphs that the results using the BIE code presented here are significantly more accurate. They are

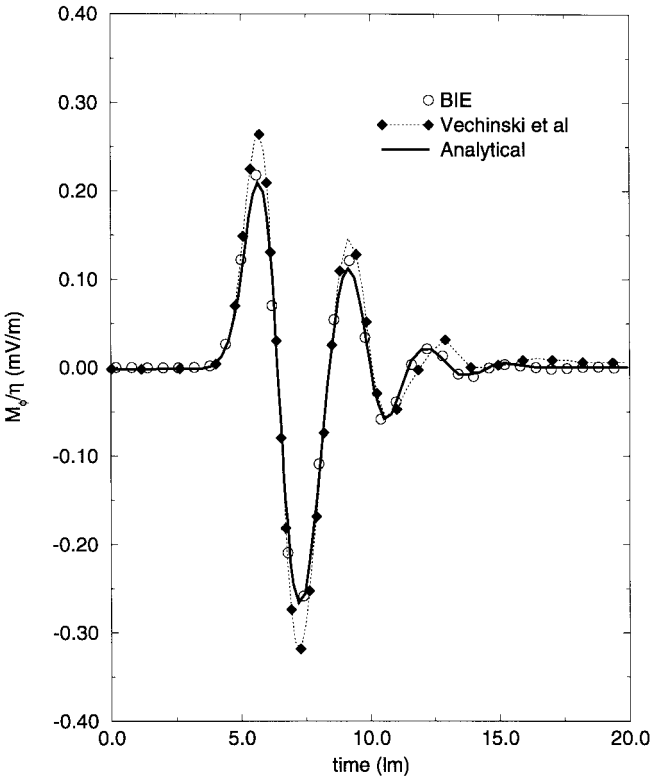

Fig. 2. The equivalent surface magnetic current, M_ϕ at $\theta = 90°$, $\phi = 0°$ for pulsed excitation of a sphere. Comparison is made between the present code, the results of Vechinski *et al*. [8], and the analytical solution.

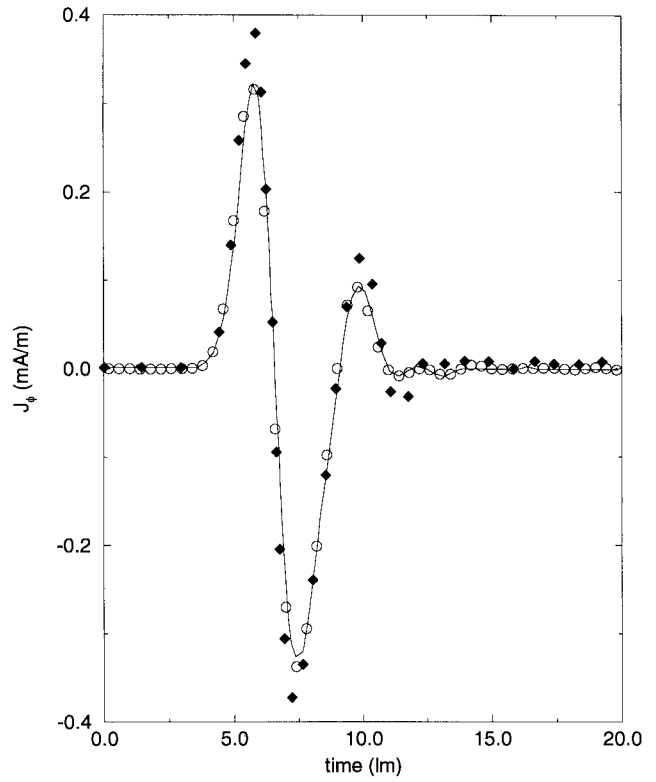

Fig. 3. The equivalent surface electric current J_ϕ at $\theta = 90°$, $\phi = 90°$ for pulsed excitation of a sphere. The present results and those of Vechinski *et al*. [8] are compared with the analytical solution.

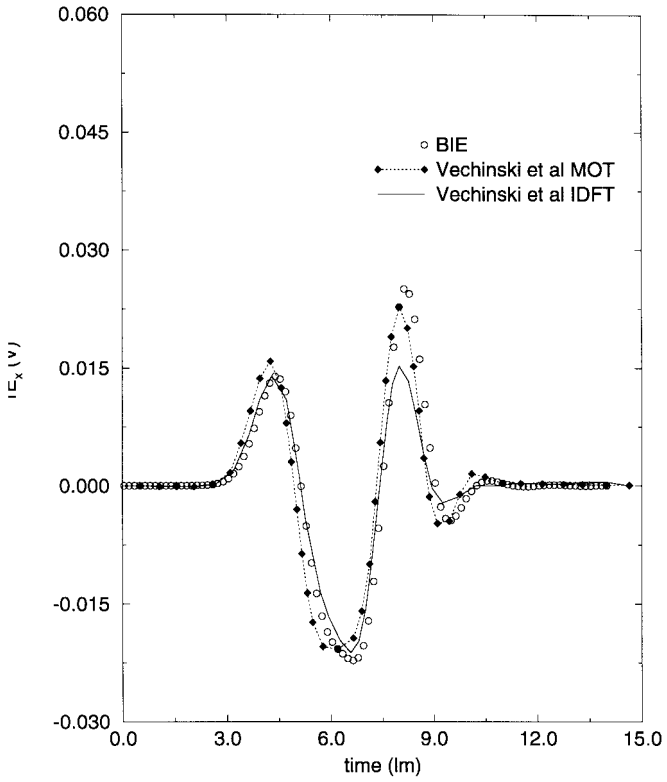

Fig. 4. Backscattered x component of E field from a cube. The present results are compared with those of Vechinski *et al*. [8].

not shown here, but good agreement was similarly obtained for other orientations.

B. Cube

The results of transient scattering from a cube have also been published by Vechinski *et al*. [8] using the incident wave described in Section III-A. The cube is centered on the origin, has a side of unit length and has the same material properties as the sphere. Meshes of 98 and 290 nodes, respectively, were used by us with virtually indistinguishable results. The backscattered x-directed component of the E field is shown in Fig. 4 together with the results due to Vechinski *et al*., which comprise an inverse discrete Fourier transform (IDFT) of a frequency-domain result and a marching on in time (MOT) result. (Note that these results have been obtained by us directly from the figures printed in their paper and are subject to some error from this.)

The results are in reasonable agreement with Vechinksi *et al*., though some differences are apparent, notably the late peak, which is in better agreement with the MOT calculation than the IDFT result. The reasons for this are unknown.

C. Almond

The NASA almond [10] presents a challenging application for modeling: it has a very low head-on radar cross section (RCS), smoothly curved geometry, and a sharp tip. The RCS is dominated by creeping waves and so its computation can be adversely affected by geometric distortions such as "staircasing" or "facetting" produced by some modeling techniques. While measurements on only a perfectly conducting

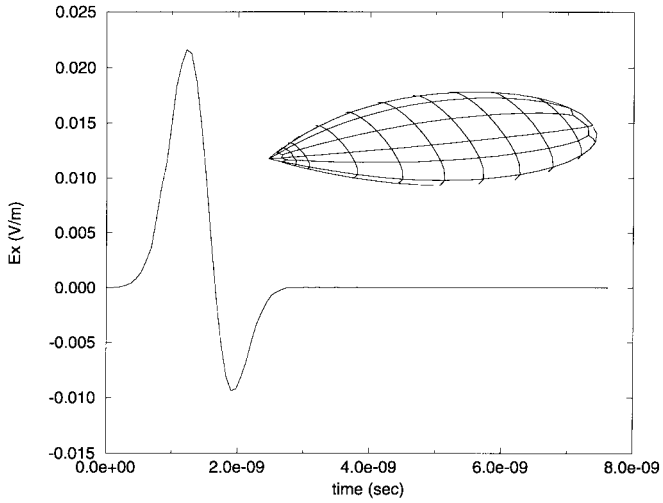

Fig. 5. Interior surface electric field magnitude at a point $(-0.077, -0.02, -0.01)$ on the almond for pulsed excitation. Inset: The mesh of the NASA almond [10], comprising 132 quadratic quadrilateral elements.

version have been published, it thus, nonetheless, provides an interesting challenge for the present time-domain dielectric treatment.

The almond mesh comprising of 132 elements is shown inset in Fig. 4 and is 0.252 m long. Material properties the same as the Vechinski *et al*. [8] sphere and cube results cited above $(\varepsilon_{r2} = 2.0, \mu_{r2} = 1.0)$ were used. The precise configuration of this problem is described elsewhere [10].

It can be seen that near the tip the mesh is refined to accurately model the geometry. An explicit method would require a time-step size smaller than the temporal separation of the nodes on the smallest element. The implicit method presented here has no such limit and, thus, uses fewer (larger) time steps, reducing computational costs.

Fig. 5 shows the x component of the interior surface electric field at $(-0.077, -0.02, -0.01)$ when the almond is illuminated with a Gaussian pulse of half-height full-width equal to 0.127 m, traveling in the x direction and z polarized. The stability of the field for many transit times is clear.

A comparison between the time domain code and a frequency-domain code [18] is presented in Fig. 6. A harmonic excitation is used in the time-domain code, with the harmonic incident wave x directed and polarized in the z direction, and of frequency 1.19 GHz. The almond is approximately one wavelength long at this frequency. The quasi-steady-state (after several transit times) time-domain solution is extracted for comparison with the frequency-domain code solution. The results show the variation of the magnitude of the x and z components of the interior electric field plotted against the x coordinate of a line of nodes from the tip to tail, across the "top" of the almond. The upper and lower lines represent the z and x components, respectively. Good agreement between the time- and frequency-domain codes is apparent.

D. Costs and Timings

We will quote here actual run times and storage needs for a particular case, along with an indication of how these will scale with problem electrical size.

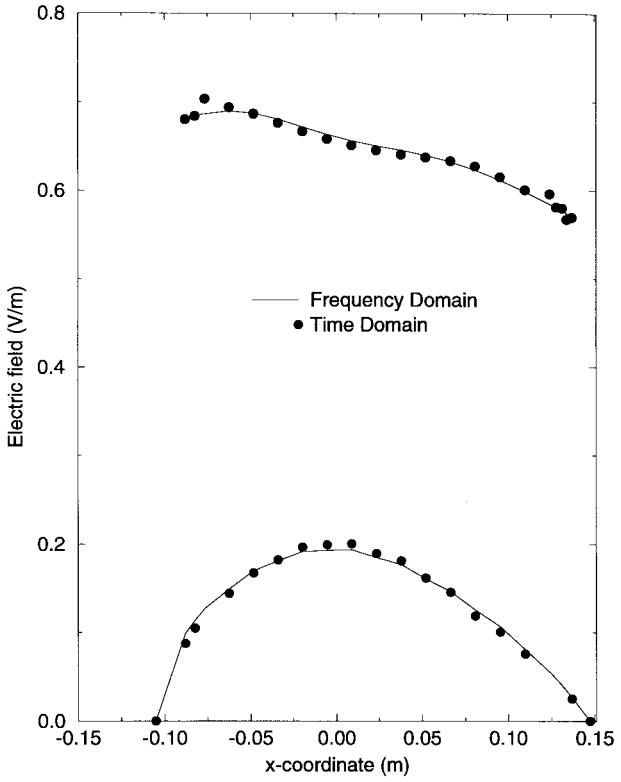

Fig. 6. The magnitude of the x and z components of the interior surface electric field along the top of the almond (at $y = 0$, $z \geq 0$ for x varying along the length of the almond). Comparison between time-domain and frequency-domain code results. Upper and lower lines represent the z and x components, respectively.

For the sphere discretized with 98 nodes, 21 Mb was required with an elapsed run time of 25 s on a DEC Alphastation 255 with a 233-MHz processor. Asymptotically, storage requirements scale with electrical size to the fourth power and run time to the fifth, although on this small problem some lower scaling cost components actually dominate.

Storage can quickly become prohibitive. An alternative approach is to recalculate all the coefficients of (21) at each timestep, as they are needed. This occasions a one-off increase in operations by a factor of about 20. In exchange, the dominant storage requirement is eliminated. Using such an approach, the same case had storage and run time requirements of 6 Mb and 34 min, respectively. The reason for the factor of $\sim$100 increase in run time in this example is because this is a small problem where the single "frequency to the fourth" matrix formation dominates the cost of the "in-core" case. This ceases to be so for larger problems, where the multiplier is the factor of 20 mentioned earlier. Storage now scales with electrical size cubed (the field histories) and time (still) with the fifth power. Electrical target sizes are primarily constrained by what constitutes an acceptable run time.

IV. Conclusion

We have demonstrated the application of curvilinear, isoparametric modeling to scattering from dielectric targets in contrast to the flat facetting and constant or linear element treatments normally employed. Additionally, an implicit treatment is used. This seems to provide stability without resorting to the averaging processes normally found necessary. Further, by permitting free choice of timestep, it avoids the large increases in computational cost attendant on constraining the timestep to be smaller than the smallest nodal spacing. Where we can compare, more accurate results than those published elsewhere are obtained.

References

[1] E. K. Miller, "A selective survey of computational electromagnetics," *IEEE Trans. Antennas Propagat.*, vol. 36, pp. 1281–1305, Sept. 1988.
[2] A. J. Poggio and E. K. Miller, "Integral equation methods of three-dimensional scattering problems," in *Computer Techniques for Electromagnetics*, R. Mittra, Ed. Oxford, U.K.: Pergamon, 1973, pp. 159–265.
[3] S. M. Rao and D. R. Wilton, "Transient scattering by conducting surfaces of arbitrary shape," *IEEE Trans. Antennas Propagat.*, vol. 39, pp. 56–61, Jan. 1991.
[4] B. P. Rynne, "Time-domain scattering from arbitrary surfaces using the electric field integral equation," *Electromagn. Waves Applicat.*, vol. 5, pp. 93–112, 1991.
[5] M. J. Bluck and S. P. Walker, "Time-domain BIE analysis of large three-dimensional electromagnetic scattering problems," *IEEE Trans. Antennas Propagat.*, vol. 45, pp. 894–901, May 1997.
[6] H. Mieras and C. L. Bennett, "Space–time integral equation approach to dielectric targets," *IEEE Trans. Antennas Propagat.*, vol. AP-30, pp. 2–9, Jan. 1982.
[7] B. P. Rynne, "Time domain scattering from dielectric bodies," *Electromagn.*, vol. 14, pp. 181–193, 1994.
[8] D. A. Vechinski, S. M. Rao, and T. K. Sarkar, "Transient scattering from three-dimensional arbitrary shaped dielectric bodies," *J. Opt. Soc. Amer.*, vol. 11, pp. 1458–1470, 1994.
[9] S. M. Rao, D. R. Wilton, and A. W. Glisson, "Electromagnetic scattering by surfaces of arbitrary shape," *IEEE Trans. Antennas Propagat.*, vol. AP-30, pp. 409–418, Mar. 1982.
[10] A. C. Woo, H. T. G. Wang, and M. J. Schuh, "Benchmark radar targets for the validation of computational electromagnetics programs," *IEEE Antennas Propagat. Mag.*, vol. 35, pp. 84–89, Feb. 1993.
[11] R. F. Harrington, *Field Computation by Moment Methods*. New York: MacMillan, 1968.
[12] E. Marx, "Integral equation for scattering by a dielectric," *IEEE Trans. Antennas Propagat.*, vol. AP-32, pp. 166–172, Feb. 1984.
[13] J. C. Lachat and J. O. Watson, "Effective numerical treatment of boundary integral equations: A formulation for three-dimensional elastostatics," *Int. J. Numer. Methods Eng.*, vol. 10, pp. 991–1005, 1976.
[14] M. J. Bluck, M. D. Pocock, and S. P. Walker, "An accurate method for the calculation of singular integrals arising in time-domain integral equation analysis of electromagnetic scattering," *IEEE Trans. Antennas Propagat.*, vol. 45, pp. 1793–1798, Dec. 1997.
[15] M. J. Bluck, "Integral equation methods for transient wave propagation," Ph.D. dissertation, Univ. London, U.K., 1993.
[16] M. J. Bluck and S. P. Walker, "Analysis of three dimensional transient acoustic wave propagation using the boundary integral equation method," *Int. J. Numer. Methods Eng.*, vol. 39, pp. 1419–1431, 1996.
[17] S. P. Walker and C. Y. Leung, "Parallel computation of integral equation methods for three dimensional transient wave propagation," *Commun. Numer. Methods Eng.*, vol. 11, pp. 515–524, 1995.
[18] M. D. Pocock and S. P. Walker, "Radar cross Section prediction using boundary integral equation methods with isoparametric quadratic surface modeling and iterative solvers," *Electromagn.*, vol. 16, pp. 651–669, 1996.

Martin D. Pocock received the B.Eng. degree in electrical and electronic engineering and the Ph.D. degree, both from Imperial College, London, U.K., in 1989 and 1994, respectively.

During 1990, he worked in the radiation laboratory of Thorn EMI Electronics Ltd., Middlesex, U.K. From 1990 to 1997 he was with the Computational Mechanics Section of the Mechanical Engineering Department, Imperial College. In 1997 he joined the Fraser Nash Consultancy, Surrey, U.K., working on computational electromagnetics problems.

Michael J. Bluck received the B.Sc. degree in mathematics from the University of Kent, Canterbury, U.K., in 1988, and the Ph.D. degree from Imperial College, U.K., in 1993, for work on the development of time-domain integral equation methods.

He was with the Electricity Council Research Centre from 1988 to 1990. He is currently a member of the Computational Mechanics Section of the Mechanical Engineering Department of Imperial College and has interests in application and development of computational techniques for wave scattering, with particular emphasis on time-domain integral equation methods.

Simon P. Walker received the B.Sc. and Ph.D. degrees from Imperial College, London, U.K., in 1977 and 1980, respectively.

Following periods working with Shell International (Holland and Canada) and the United Kingdom Atomic Energy Authority, he returned to Imperial College in 1984, where he is Reader in Computational Mechanics. His group in the Computational Mechanics Section has interests in application and development of computational techniques for large scattering analyses, with particular emphasis on integral equation methods for radar cross section.